REPORT DOCUMENTATION PAGE

Form Approved
OMB NO. 0704-0188

1. AGENCY USE ONLY (Leave Blank)	2. REPORT DATE	3. REPORT TYPE AND DATES COVERED
	31 Jul 2000	Final Progress: 1 Apr 1996 - 30 Apr 2000

4. TITLE AND SUBTITLE
Intrinsic Burning Behavior and Flame Structure Diagnostics of Liquid Propellants

5. FUNDING NUMBERS
DAAH04-96-1-0054

6. AUTHOR(S)
K. K. Kuo, Y. P. Chang, and E. Boyer

7. PERFORMING ORGANIZATION NAME(S) AND ADDRESS(ES)
The Pennsylvania State University
Department of Mechanical and Nuclear Engineering
University Park, PA 16802

8. PERFORMING ORGANIZATION REPORT NUMBER

9. SPONSORING / MONITORING AGENCY NAME(S) AND ADDRESS(ES)
U. S. Army Research Office
P.O. Box 12211
Research Triangle Park, NC 27709-2211

10. SPONSORING / MONITORING AGENCY REPORT NUMBER
ARO 34839.3-EG

11. SUPPLEMENTARY NOTES
The views, opinions and/or findings contained in this report are those of the author(s) and should not be construed as an official Department of the Army position, policy or decision, unless so designated by other documentation.

12 a. DISTRIBUTION / AVAILABILITY STATEMENT
Approved for public release; distribution unlimited.

12 b. DISTRIBUTION CODE

13. ABSTRACT (Maximum 200 words)

From the combustion study of HAN-based liquid monopropellants, XM46 was found to exhibit unconventional characteristics with flashback behavior and negative pressure exponent. These characteristics are believed to be caused by the complex physical and chemical process occurring in condensed-phase region. The intrinsic burning rates of XM46 increased with pressure when $P < 7$ MPa, decreased for $7 < P < 28$ MPa, exhibited a hump-like shape when $28 < P < 80$ MPa, and increased again when $P > 80$ MPa. Luminous flame was observed only when $P > 28$ MPa. TEAN participates in the decomposition reactions of XM46 initiated in the liquid phase, producing dark-colored gaseous products (including NO_2 and large carbon-containing species) at T~300 °C. The major pyrolysis products of XM46 observed from a specially designed pyrolyzer were NO, N_2O, N_2, CO_2, CO, H_2O, HCN, and C_2H_4 for $130 < T < 540$ °C. Water evaporation appears to affect XM46 combustion, since the latent heat is about the same as the activation energies of HAN and TEAN and the heat release in the decomposition zone. The fuel ingredient in HAN-based propellant has a significant effect on burning characteristics, as demonstrated by the replacement of TEAN with glycine.

14. SUBJECT TERMS	15. NUMBER OF PAGES
XM46 liquid propellant, monopropellant, combustion, pyrolysis, chemical kinetics, decomposition, flashback, HAN, TEAN, glycine, liquid propellant strand burner, ultra high pressure strand burner, burn rate	25
	16. PRICE CODE

17. SECURITY CLASSIFICATION OR REPORT	18. SECURITY CLASSIFICATION ON THIS PAGE	19. SECURITY CLASSIFICATION OF ABSTRACT	20. LIMITATION OF ABSTRACT
UNCLASSIFIED	UNCLASSIFIED	UNCLASSIFIED	UL

NSN 7540-01-280-5500

Standard Form 298 (Rev.2-89)
Prescribed by ANSI Std. 239-18
298-102

20001124 014

Table of Contents

Table of Figures

1 Statement of Problem

Since its production, XM46 liquid propellant, consisting of hydroxylammonium nitrate [HAN, NH_3OHNO_3, 60.8% by wt.], triethanol ammonium nitrate [TEAN, $(HOCH_2CH_2)_3NHNO_3$, 19.2%], and water [20%], has been of great interest to the U.S. Army because of its desirable features such as high energy density and relatively low flame temperature. Numerous studies have been conducted to understand the complex properties of this liquid monopropellant. In this investigation, the intrinsic burning rates of XM46 were studied and different diagnostic techniques were applied to the study of its combustion behavior. Both traditional static burning tests in tubes and feeding tests were performed. However, XM46 exhibits many unconventional characteristics. First, the burning rate versus pressure curve has regions with positive and negative pressure exponents. Second, when tested with feeding techniques, XM46 exhibits flashback characteristics even with a relatively high feeding speed (~ 15 in/s). The reaction front keeps regressing into the feeding tube at a nearly constant speed at all the pressures and feeding speeds tested. Therefore, it is desirable to characterize the conditions of the flashback, and identify possible reasons. Through an in depth examination, the possible controlling parameters of the burning rate were identified and investigated. Also, to study the effect of fuel components on the characteristics of the HAN-based liquid propellants, including the burning rate and flame structure, another liquid propellant blend with glycine (H_2-NCH_2-COOH) instead of TEAN as the fuel component was tested.

2 Method of Approach

Two strand burners – the liquid propellant strand burner (LPSB) and an ultra-high pressure strand burner (UHPSB) were used to test the combustion characteristics of HAN-based liquid propellants. The LPSB contains an accurate liquid feeding system, enabling the stabilization of the flame at a fixed location and observation and measurement of combustion phenomena through the optically-accessible windows. For testing at pressures higher than 35 MPa, the UHPSB was used, up to a maximum pressure of 207 MPa. A Shimadzu QP-5000 Gas Chromatograph/Mass Spectrometer (GC/MS) system coupled with a Shimadzu PYR-4A high-temperature pyrolyzer was used to identify and quantify the pyrolysis species of propellants at temperature of interest

2.1 LPSB

Figure 1 is a schematic diagram of the LPSB. As shown, the LP is fed by a piston through a feed line to a transparent tube contained within a test chamber. The chamber is pressurized with nitrogen drawn from an ultra-high-pressure compressor and reservoir system, which can store gas at pressures up to 207 MPa.

Four windows on the combustion chamber allow visual monitoring as well as optical diagnostics such as UV/Visible absorption spectroscopy. Additionally, there are numerous ports for pressure transducers and thermocouple placement throughout the test rig. Optional heat exchangers surrounding the propellant feed lines can be used with a constant-temperature bath to precondition the liquid propellant to temperatures between –80 and 45 °C. Using this system,

the combustion behavior of an LP can be studied as a function of initial temperature. Static tests and feeding tests were performed using this test rig.

Both quartz tubes and combustible straws were used to measure burn rates in static tests. The inside diameter of the quartz tubes was 7 mm; the length was approximately 75 mm. Combustible straws were fabricated from wax paper wrapped twice around a 6.5-mm mandrel. A very thin layer of contact adhesive was used to seal the layers together. Three breakwires mounted across the straws were used to measure the regression rate. Purge flow from the base prevented flame-spreading down the straw sides and kept the chamber clear of smoke. The quartz tube or combustible straw was mounted on the center of the base insert block to the LPSB, in place of the feeding tube. The liquid strand was totally visible through the viewing window to allow visual observation and analysis.

In feeding tests, liquid propellants were fed up through a tube in order to establish a stable flame at the exit port of the tube. Once a stable flame was established, one could deduce burning rate from the preset feeding speed. To prevent the flame from propagating all the way into the LP reservoir, the feed line was designed to include a high-pressure purge system. If the flame proceeded into the feed line, the feeding action was halted and high-pressure nitrogen was introduced from the flame extinguisher line through a check valve into the LP feed line beneath the base of the test chamber, purging the reacting propellant from the system before it could affect the reservoir.

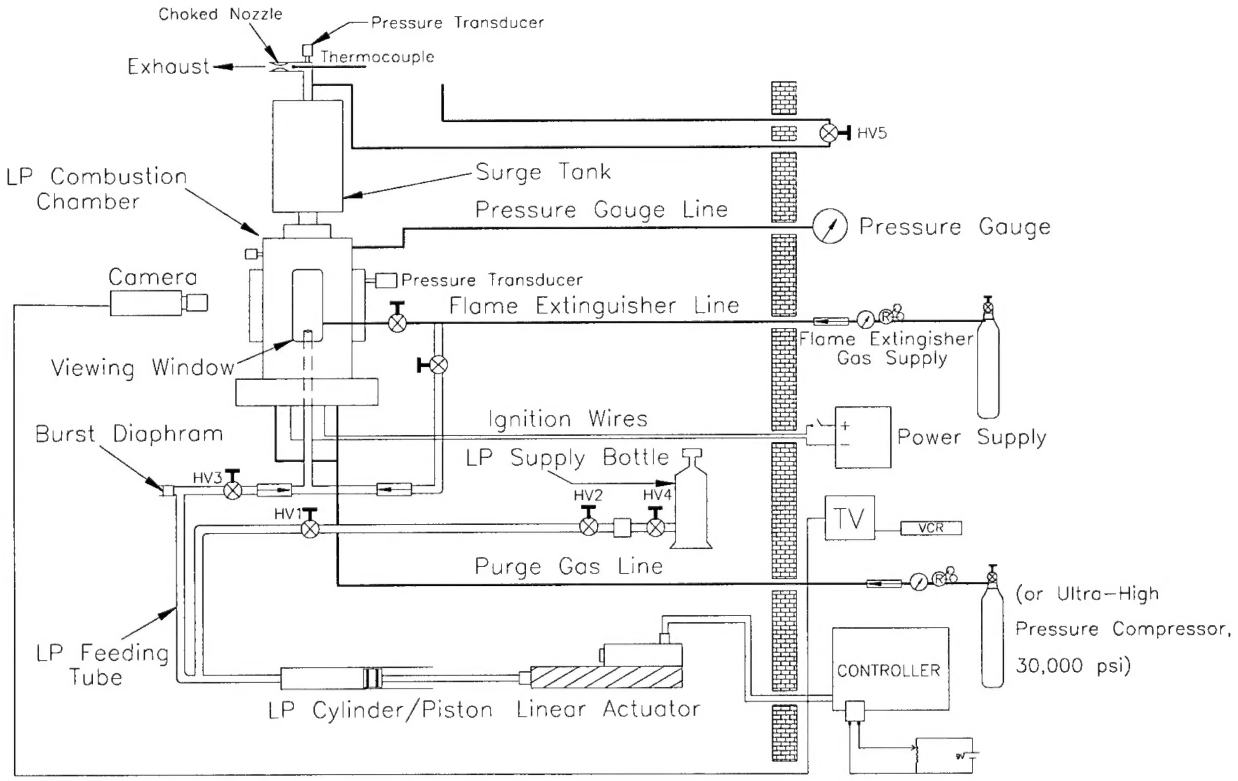

Figure 1. Schematic diagram of liquid propellant strand burner used in combustion study.

2.2 UHPSB

Conventional vented strand burners generally have pressure limits of less than 70 MPa (~10,000 psi). However, pressures generated inside gun chambers are much higher, possibly exceeding 700 MPa (~100,000 psi). Gaining more knowledge of high-pressure reaction mechanisms can also be useful in understanding detonation initiation and reaction processes for energetic substances. The optically accessible LPSB used in this study was limited to pressures less than 35 MPa by the windows, so in order to examine the combustion behavior at high pressures, an ultra-high pressure strand burner (UHPSB) was designed, constructed, and tested.

The UHPSB and its remote control system comprise a unique facility established at the High Pressure Combustion Laboratory (HPCL) of Penn State University that allows regression rates of strand propellants to be measured at pressures up to 207 MPa (30,000 psi). Two solid or liquid strands up to 65 mm long can be tested simultaneously to minimize gas usage and maximize data return. Adapted from an existing high-pressure compressor storage tank with a large internal volume, the UHPSB provides a nearly constant-pressure testing environment.

Liquid or gelled propellant strands can be contained in either a quartz tube (for simplicity) or combustible straws (to minimize heat loss and confinement effects). To pass ignition power and diagnostic signals through the high-pressure chamber wall, a custom-made 8-wire electrical feedthrough was utilized. The control panel allows operation and observation of a number of important functions from a remote site, including:

- compressor power control
- exhaust valve actuation
- electrical continuity test on TC/BW/ignition
- trigger output from ignition switch for data acquisition system activation
- Variac or DC power source control for igniter power input

The burning of the propellant was monitored using multiple breakwires. Segments of Bussman 0.25-amp fuse wire were utilized as break wires threaded through the propellant strands. Burning rate was deduced by measuring the time delay between burnthrough of adjacent wires. For solid strands, up to 4 holes were drilled or punched at known intervals, and the break wires were passed through these holes. Break wire holes in combustible straws or quartz tubes were sealed with a dot of epoxy to contain liquid propellants. Thermocouple mounting was similar to the break wire mounting. A total of three thermocouples (TCs), or up to four break wires (BWs) per sample can be monitored using this setup. Also, the number of break wires can be increased with simple modifications to the sample base. As configured, the UHPSB used a nichrome hot-wire ignition system. Electrical energy was supplied by either a Variac or DC power source at the control panel. In some cases, a solid propellant initiator consisting of an easily-ignitable solid propellant disc (e.g., NOSOL-363) was attached to the nichrome wire to ensure uniform ignition. In addition, the system can be easily reconfigured to use any other type of initiator or electrically actuated igniter.

Since the test chamber was adapted from a high-pressure compressor storage tank with a length of approximately 6 feet and a 4-inch inside diameter, the internal volume is very large. Therefore, there is negligible pressure change due to product gases released during the combustion event. The high-pressure gas environment for combustion was determined by the

gas input source to the compressor. The environment was generally nitrogen, but other gases such as air or argon could easily be substituted.

A schematic diagram of the UHPSB is shown in Fig. 1. It can be seen that the controls and data acquisition systems are located in another building apart from the one containing the UHPSB test chamber. Both the compressor and the exhaust solenoid valve (SV1) can be remotely operated to increase or decrease the chamber pressure to the desired level. To run an experiment, the igniter power input is then set, and the test triggered.

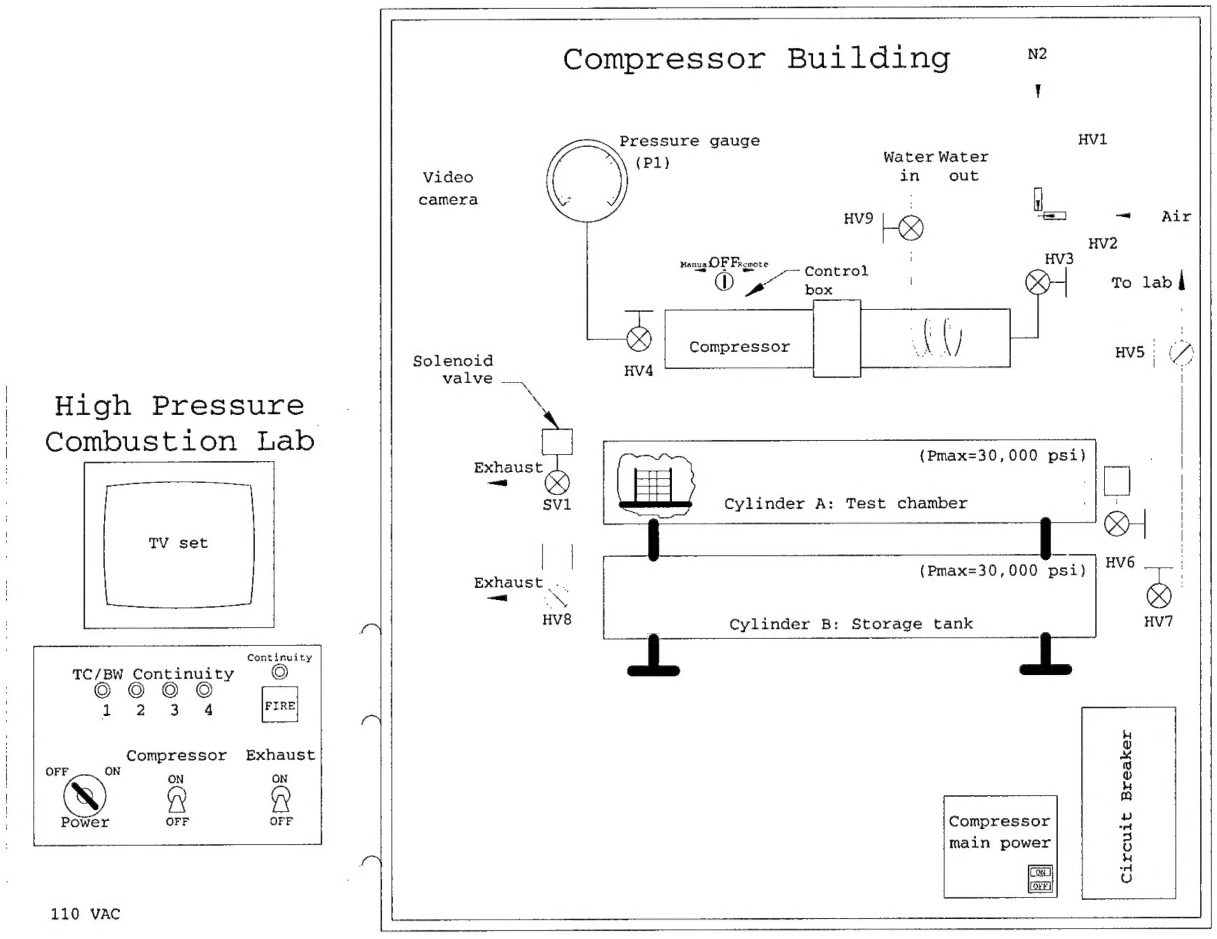

Figure 2. Schematic diagram of UHPSB.

2.3 GC/MS with Flash Pyrolyzer

A Shimadzu QP-5000 Gas Chromatograph/Mass Spectrometer (GC/MS) system coupled with a Shimadzu PYR-4A high-temperature pyrolyzer was used to identify and quantify the pyrolysis species of propellants at temperature of interest. A small amount of sample was placed in a platinum cup and dropped into the pyrolyzer at a preset temperature. The maximum temperature of the pyrolyzer is 800°C. The gas evolved was carried into the GC sub-system by helium, where the different compounds in the gas were separated by the capillary column. The separated compounds passed through the transfer interface and went into the MS sub-system. The sub-system ionized and/or fragmented the compounds by electron beam, and scanned through the

specified mass-to-charge ratio (M/Z) range to determine the mass spectrum of the compound. The MS sub-system can scan the ions with M/Z between 10 and 700 at a maximum scanning rate of 6,000 amu/s. The mass spectrum measured was compared with spectra of known substances by software to identify the species. Each compound was quantified by integrating the area under its chromatograph peak and comparing the area with the calibration constant obtained using the pure substance.

3 Review of HAN-based Liquid Propellant Kinetics

Different stoichiometries of HAN decomposition have been reported by different authors:

$$7HAN \rightarrow 4N_2O + N_2 + 4HNO_3 + 12H_2O \quad \textbf{(R 1)}^{1,2}$$

$$4\ HAN \rightarrow 3\ N_2O + 7\ H_2O + 2\ HNO_3 \quad \textbf{(R 2)}^{3}$$

$$4\ HAN \rightarrow 3.2\ N_2O + 7.2\ H_2O + 1.6\ HNO_3 + 0.4\ O_2 \quad \textbf{(R 3)}^{3}$$

The above variations show that the chemical kinetics of HAN decomposition is extremely complicated; therefore, the final product composition will change with respect to different test conditions, such as pressure, heating rate, salt concentration, etc.

Klein[1] has developed a detailed 3-stage decomposition process of HAN. The initiating stage is a proton transfer that occurs in the condensed phase as the HAN produces hydroxylamine (NH_2OH) and nitric acid. Further breakdown of these compounds results in HNO and HONO production. These reactive species are important in the second stage, which is characterized by the rapid depletion of HAN, and production of more nitric acid and HONO as well as N_2O, H_2O and NO.

In the pyrolysis study by Lee and Thynell[4], the product species of decomposed HAN was measured using rapid thermolysis/FTIR. HAN was pyrolyzed at temperatures from 120 to 180 °C. Results showed the major species to consist of H_2O, N_2O, NO, HNO_3, and NO_2. These species may well represent the condensed phase pyrolysis products near the initial pyrolysis front around 120 °C in the subsurface region. A more detailed three-step mechanism was proposed based upon Klein's kinetics.

Cronin and Brill[5] examined the pyrolysis products of HAN, TEAN, and LGP1845 (3% less water than XM46) by heating samples on a nichrome ribbon filament at rates from 20-400 °C/s. They found four main events during the process. First, water evaporates and concentrates the sample. Second, proton transfer between the cation and anion of HAN initiates the decomposition of HAN. This happens at around 160-170°C. The third step is the partial decomposition of TEAN at around 240-250 °C. The last one is the ignition of the sample. Increasing the heating rate speeded the reaction through the steps described above toward combustion. Increasing the pressure reduced the water departure amount by raising the evaporation temperature, and seemed to cause the HAN decomposition temperature to go toward the TEAN-oxidizer exotherm.

Beyer[6] used a shock tube to measure the activation energy of TEAN powder under oxygen/Ar and nitrous oxide/Ar environments. The activation energies measured under oxygen/Ar and nitrous oxide/Ar environment is 9.6 and 16.3 kcal/mol (40.3 and 68.5 kJ/mol), respectively. The author suggested that the activation energy measured was largely due to the melting of TEAN; that is, the melting might be the rate-limiting step. He also suggested that TEAN reacts rapidly

after it is melted. It is interesting to note that the activation energy of solid TEAN provided by Beyer is very close to what reported for aqueous HAN.[7]

As summarized by Thynell et al.[8], the reaction kinetics of HAN decomposition start with proton transfer:

$$NH_3OH^+–NO_3^- \leftrightarrow NH_3O + HNO_3 \quad \textbf{(R 4)}$$

The ammonium oxide is generally unstable; in dilute solutions, it is quickly rearranged into hydroxyl amine:

$$NH_3^+O^- \rightarrow N\,H_2OH \quad \textbf{(R 5)}$$

The nitric acid can further decompose to nitronium ion and hydroxyl ion:

$$HNO_3 \leftrightarrow NO_2^+ + OH^- \quad \textbf{(R 6)}$$

The reaction between the ammonium oxide and nitronium ion can form nitrous acid:

$$NH_3O + NO_2^+ \rightarrow H_2NO^+ + HNO_2 \quad \textbf{(R 7)}$$

The hydroxyl ion initiates the formation of nitroxyl (HNO) via the following reaction:

$$H_2NO^+ + OH^- \rightarrow H_2O + HNO \quad \textbf{(R 8)}$$

To form N_2O, several additional reaction steps involving HAN are required. HAN can be attacked by nitrous acid by the following reaction:

$$NH_3OH^+–NO_3^- + HNO_2 \rightarrow H_3O^+ + O{=}N–NH–OH + NO_3^- \quad \textbf{(R 9)}$$

and through a simple molecular rearrangement, hyponitrous acid is formed by:

$$O{=}N–NH–OH \rightarrow HO–N{=}N–OH \text{ (hyponitrous acid)} \quad \textbf{(R 10)}$$

Hyponitrous acid is catalyzed by nitrous acid to form nitrous oxide and water:

$$HO–N{=}N–OH \rightarrow N_2O + H_2O \quad \textbf{(R 11)}$$

The reaction of HAN with HNO may cause the release of N_2 by

$$NH_3OH^+–NO_3^- + HNO \rightarrow H_3O^+ + N_2 + H_2O + NO_3^- \quad \textbf{(R 12)}$$

The production of NO and NO_2 are attributed to the following reactions:

$$HNO + HNO_2 \rightarrow 2\,NO + H_2O \quad \textbf{(R 13)}$$

$$2\,HNO_2 \rightarrow NO + NO_2 + H_2O \quad \textbf{(R 14)}$$

4 Experimental Results

4.1 XM46

The combustion characteristics of XM46 were studied using a variety of complementary methods. Regression rate in both static and feeding tests was examined. Pyrolysis products were analyzed as a function of temperature, and the thermal wave during regression was measured.

4.1.1 Burning Rate Measurements

Two different strand burner systems were used to perform both static and feeding tests over a wide range of initial pressures.

4.1.1.1 Static Tests

The burning rate vs. pressure curve for XM46 was extended up to 207 MPa with the test results obtained from the UHPSB using combustible straws. The extended results together with previous data are shown in Figure 3. The curve displays two different burning rate regimes. In the lower pressure regime (for P < 28 MPa) with no luminous flame present, the rate of regression first increases with pressure until a maximum rate of 23 cm/s is reached at 7 MPa. Beyond 7 MPa, the regression rate then decreases with increasing pressure. A localized minimum regression rate occurs near 28 MPa. In the higher pressure regime (28 < P < 200 MPa) with the presence of luminous flame, the curve exhibits a small hump before rising with respect to pressure for P > 80 MPa. It is important to note that the burning rate of neat XM46 obtained in this investigation is significantly higher than those reported by researchers at ARL[9] for slightly gelled propellants. This indicates the strong influence of gelling agents on the combustion behavior of LP. In addition, for the low-pressure regime, the PSU data are higher than those of Vosen.[10] The difference is believed to be caused by the greater heat loss from the reaction zone to the rectangular quartz channel used by Vosen.

4.1.1.2 Feeding Tests

Another phase of the study was the attempt to stabilize a flame at the top of the feeding tube by

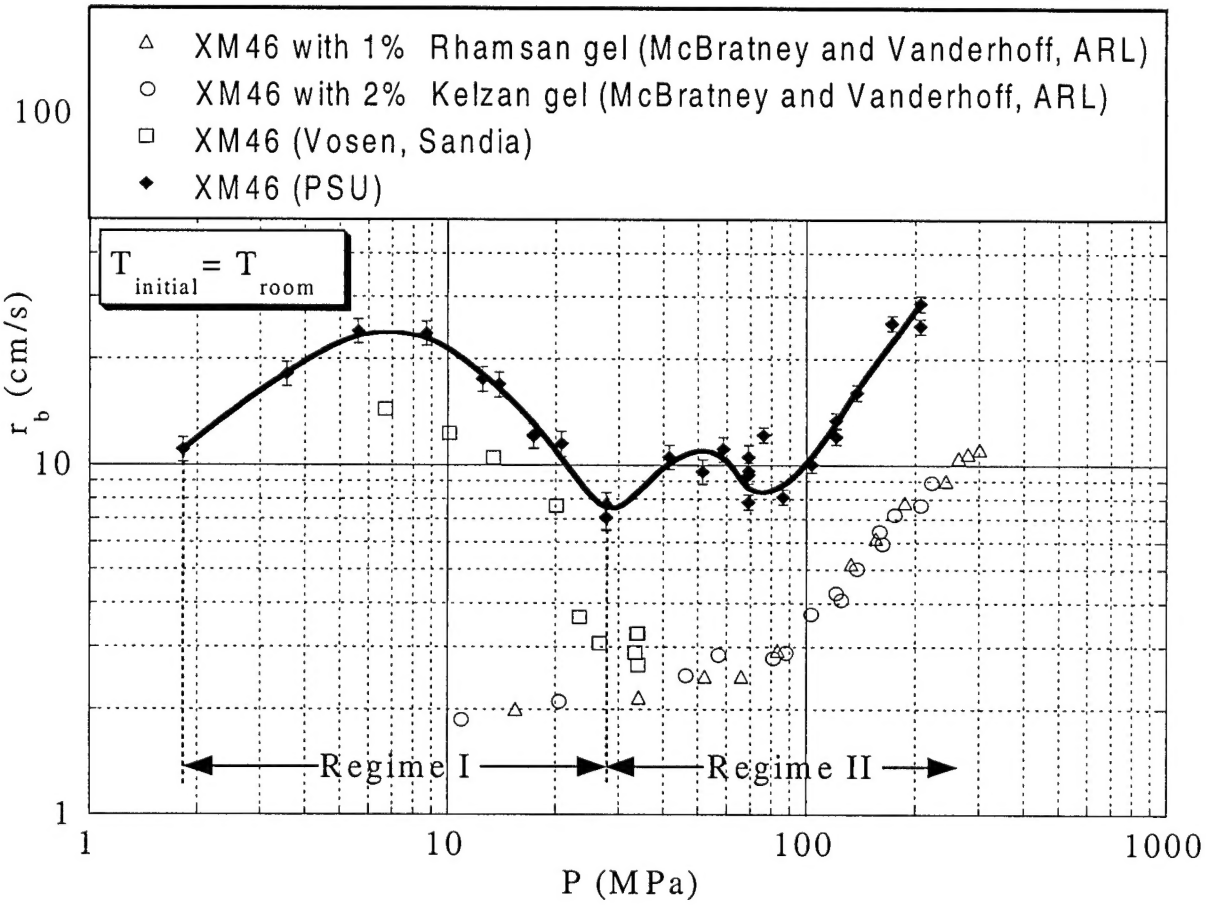

Figure 3. XM46 burning rate as function of pressure ($T=T_{room}$).

feeding the propellant into a flame at its burning rate. Using the burn rates seen in the static tube tests as the feeding rate, the "burn back" phenomenon was observed. This implies that the propellant surface regressed faster than the feeding rate. A series of tests were conducted with increasing feeding rates, however, with each case the burn back phenomenon occurred at a constant velocity down the feed line. Namely, the distance versus time plot of the regressing surface is a straight line.

The feeding rate was increased in subsequent tests from 5 to 25 cm/s for a series of initial chamber pressures (20.7, 24.1, 27.7, and 31.1 MPa). In the 27.7 MPa case, for example, the burn back always occurred at a slightly higher (~ 1.6 cm/s) regression rate than the feeding rate. Figure 4 shows the burning rate as a function of feeding rate. A data point on the 45° line would imply a stabilized flame at the exit port of the feeding tube. However, all of the data exists above this line. The slope of the curve fit for the 27.7 MPa tests data is nearly unity which implies that regardless of the propellant feeding rate, the reaction proceeds down the tube at approximately 1.6 cm/s. This value appears to be a constant liquid-phase chemical reaction-front velocity against the moving liquid surface. The data from tests at other initial chamber pressures showed very little difference in their burn back velocities into the moving liquid propellant from those of the 27.7 MPa test condition, with the exception of one data point at 20.7 MPa. Another data point at this pressure, however is located directly on the trend line amongst the other data points. Though the tube tests (unfed) showed an increase in burning rate as the pressure lowered below 28 MPa, the rate at which the burn back phenomenon occurred in feeding tests remained largely constant, even at lower pressures.

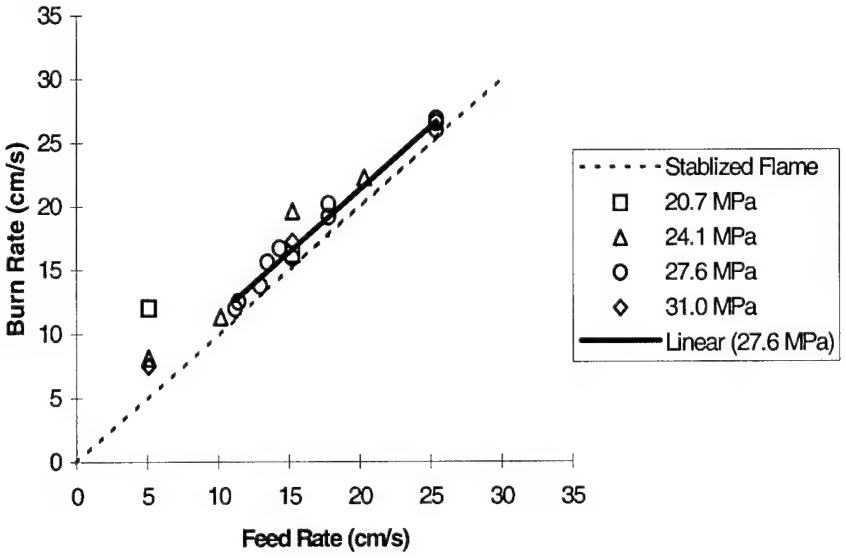

Figure 4. XM46 burn rate plotted with propellant feed rate.

Another phenomenon seen throughout the feeding tests was the presence of a black cone atop the decomposing liquid propellant surface; the black cone was not present at all in the static tube tests. The height of this cone increased as the feeding rate increased. This is clearly seen in Fig. 5a (a 7.6 cm/s feeding rate test) and Fig. 5b (a 15.2 cm/s feeding rate test). In Fig. 5a, the luminous flame initiates from the tip of the black cone. Figure 5b, however, shows that a luminous flame was not always directly in contact with the apex of this cone. As the black cone

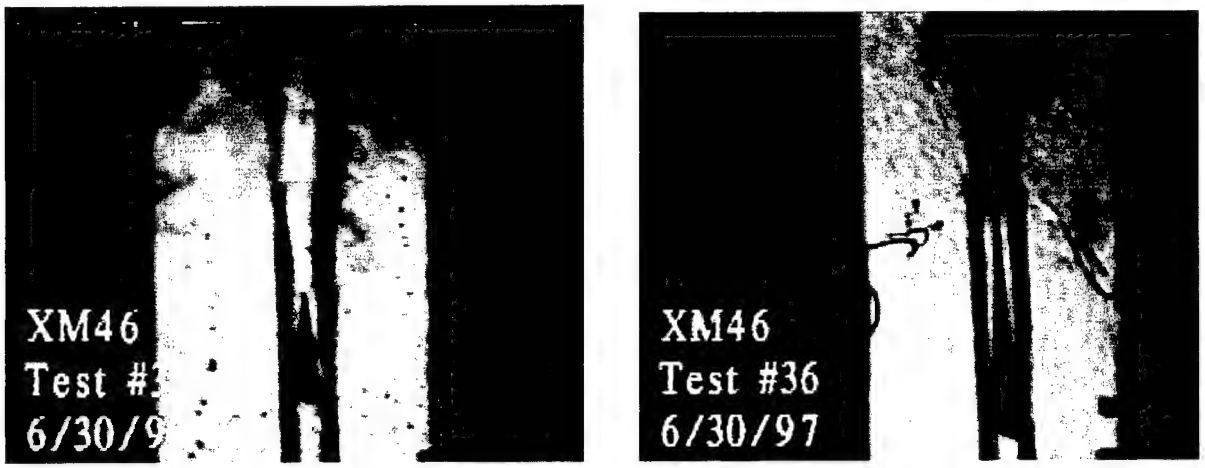

(a) (b)

Figure 5. XM46 burning at P = 27.7 MPa while fed (a) at 7.6 cm/s; (b) at 15.2 cm/s.

regressed downward with the gas-liquid interface, the flame generated in the plume above the feeding tube could propagate down to meet the tip of the cone. In most tests at higher pressures, these two inverted cones traveled together. It has also been observed that gas-liquid interface could be tilted from a horizontal position. However, the tilted plane was not always at the same orientation, which indicates it was not due to asymmetry of the feed system.

4.1.2 Temperature Measurements of the Reaction Zone

In a typical feeding test, the temperature distribution in the reaction zone of the XM46, deduced from the voltage-time trace recorded from a S-type fine-wire thermocouple, is shown in Fig.6.

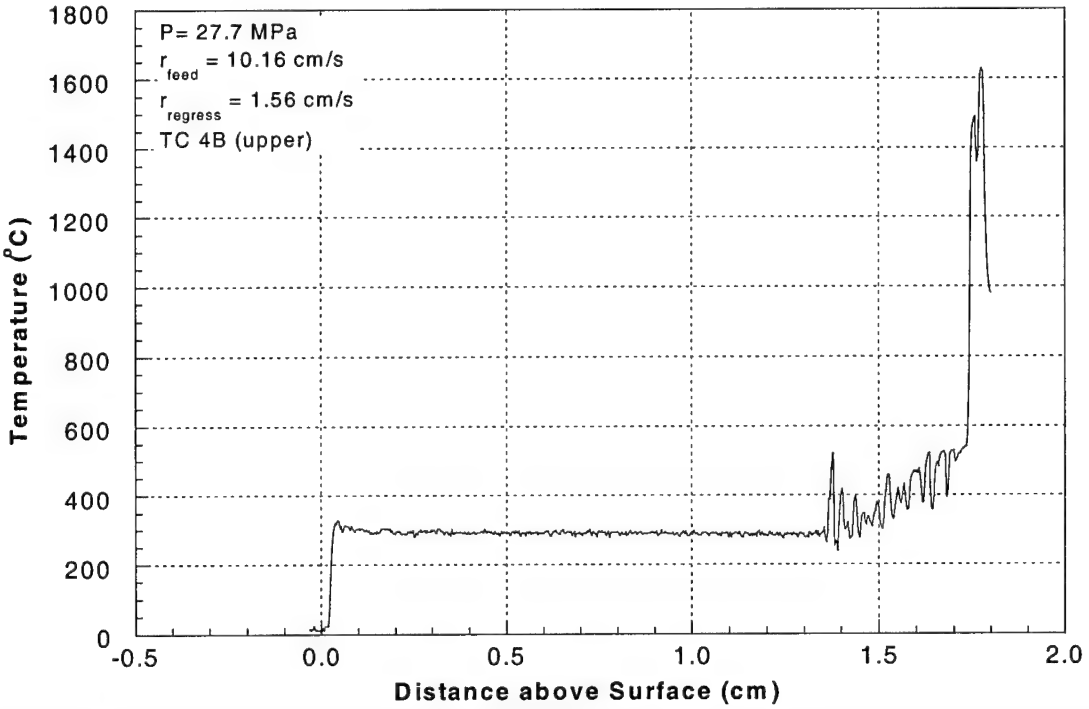

Figure 6. Temperature distribution of XM46 reaction zone under feeding condition.

The test was conducted at a pressure of 27.7 MPa, and a feeding rate of 10.16 cm/s. For this particular test condition, the cone height was 1.5-1.7 cm. Inside the cone, the temperature was around 300 °C. The temperature gradually increased in the top few millimeters, then suddenly jumped to luminous flame temperature. Oscillations starting at about 1.4 mm when the temperature begins to rise are caused by unstable fluctuations of the narrow cone tip about the small thermocouple bead.

4.1.3 Pyrolysis Products Analysis

The pyrolysis products of XM46 at different temperatures were analyzed using a Shimadzu QP-5000 GC/MS system. Figure 7 shows the amount of species (in moles) evolved from 0.2 μl of XM46 at different pyrolyzer temperatures from 130 to 540°C. The major product species detected in these tests, listed in the order of decreasing average number of moles evolved, are NO, N_2O, N_2, CO_2, CO, H_2O, HCN, and C_2H_4. As noted in the figure, the amounts of NO and HCN species are approximate values, since high concentrations of these toxic gases were not available for calibration. The appearance of NO and N_2O at temperatures as low as 130 °C is consistent with what was observed in the pyrolysis tests of HAN-water solutions by Lee and Thynell.[4] NO_2 and HNO_3 were not detectable, due to the limitations of the GC column for NO_2 and the MS detector for HNO_3. The amounts of four major HAN decomposition species, NO, N_2O, N_2, and H_2O did not change much with pyrolysis temperature. Carbon-containing species, however, showed a stronger dependence on the pyrolysis temperature. At least an order of magnitude change of the amount over the temperature range from 130 to 540 °C was observed

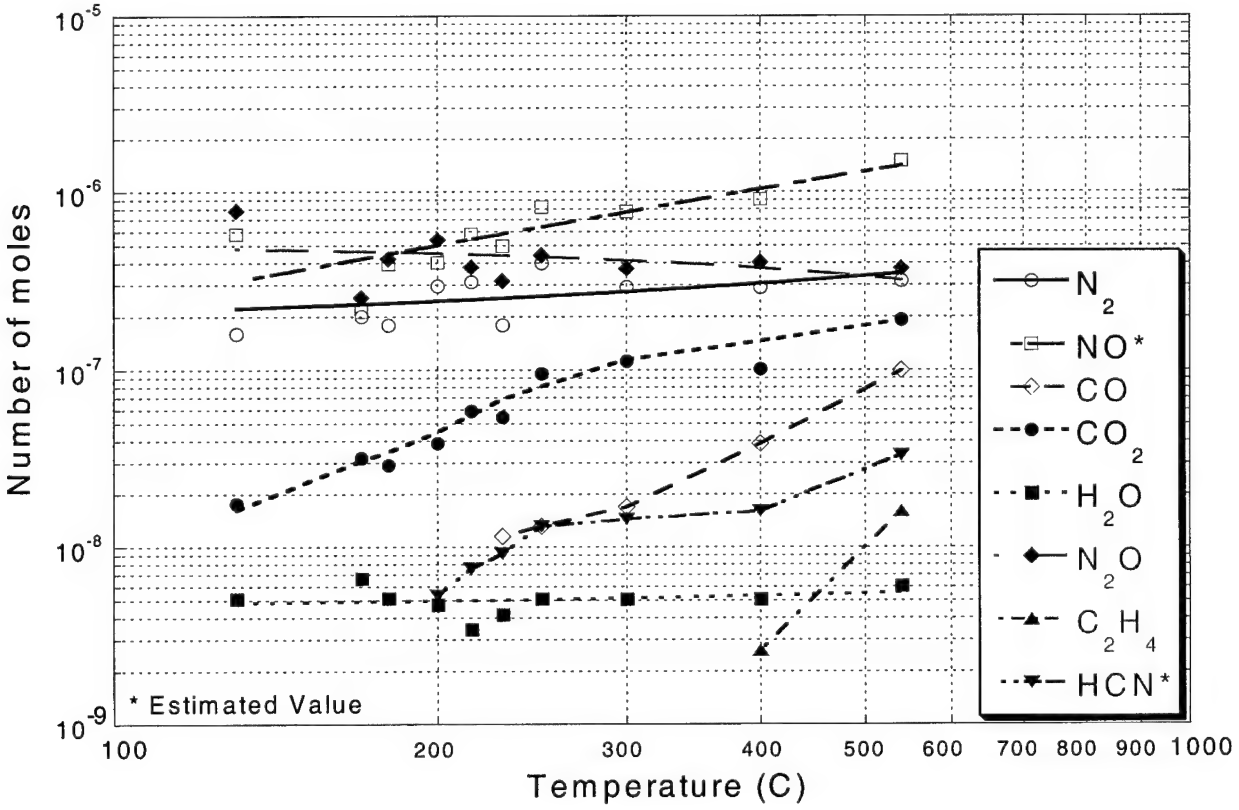

Figure 7. Mass spectrometer output for pyrolyzed XM46.

for these species. The appearance of carbon-containing species at temperatures below the generally-reported TEAN decomposition temperature of 240 to 250 °C[5] indicated the interaction between TEAN and oxidizing species generated from HAN decomposition.[11] This is also in agreement with the measurements of Lee and Litzinger.[12] As the pyrolysis temperature increased, the oxidation of TEAN by HAN decomposition products became more significant, generating more carbon-containing species. Although two of the major oxidizing species, HNO_3 and NO_2, cannot be detected, the decreasing trend of one of the detectable oxidizing species, N_2O, is consistent with the above arguments. The decreasing trend of N_2O and increasing trend of NO as the pyrolysis temperature is increased suggest multiple temperature-sensitive reaction pathways. At low temperatures, the decomposition reaction of hyponitrous acid (HO–N=N–OH) to form N_2O and water seems to be more favorable than the reactions involving H–N=O and HNO_2 to form NO and water.

4.2 Results from an Alternative HAN-Based Propellant

An alternative propellant, consisting of 60% of HAN, 14% of glycine (H_2-NCH_2-COOH), and 26% of water by weight, has been considered as a potential rocket propellant of satellite thrusters by Primex Aerospace Company. Because of the similarity of the weight percentage of HAN between XM46 and this propellant (referred as Primex propellant hereafter), tests were done on Primex propellant to compare with XM46 and to further investigate the effect of fuel components on overall performance of HAN-based liquid propellants. Tests were performed over the pressure range between 1.5 MPa and 14.5 MPa.

4.2.1 Phenomenological Description of Combustion behavior

From the combustion phenomena observed, two pressure ranges were identified. In each pressure range, the combustion of Primex propellant showed different characteristics.

4.2.1.1 Test Results for Pressures Between 1.5 and 8.8 MPa:

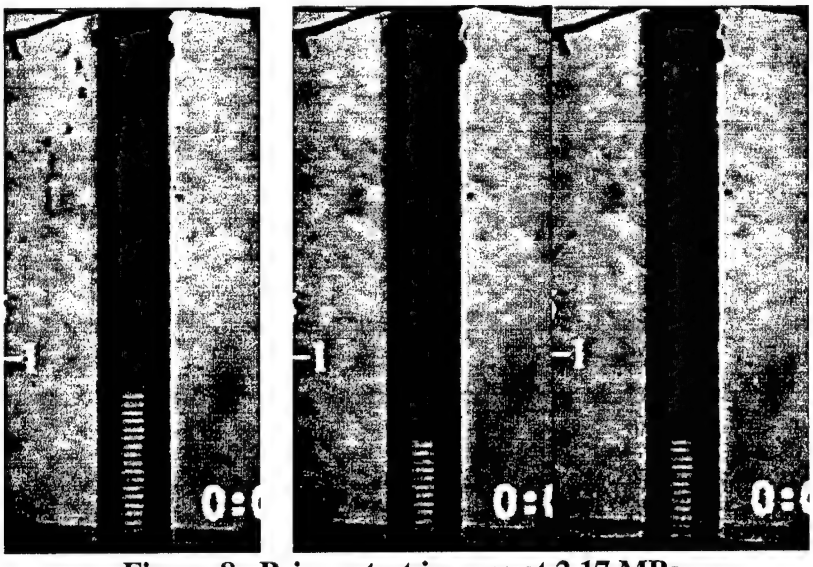

Figure 8. Primex test images at 2.17 MPa.

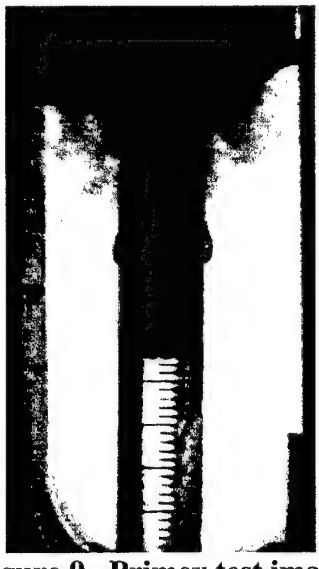

Figure 9. Primex test image at 11.8 MPa.

A typical image of the combustion event is shown in Figure 8. No luminous flame was observed in this pressure range. The reaction of the propellant formed a dark colored region on top of the regressing surface and brown-colored gas afterwards. From the left-most image, the region right beneath the dark cloud was clear, but the image of the scale was distorted. This indicated the existence of gas bubble. The bubbling at the regressing surface caused surface corrugation. Bubble size increased as the pressure decreased. On top of the regressing surface, the reaction formed a dark cloud, which is believed to be liquid with gas generating inside. Left-most image showed a gas pocket formed in the cloud region and a drop of dark-colored liquid formed due to the gas spewing. The two images right besides the first one are two consecutive frames later in the event, showing a liquid column formed by gas spewing process, and later breaking up into two drops. Due to the gas generation process, the height of the dark-colored cloud was changing with time. However, the average height of the dark-colored cloud was decreasing with increasing pressure. After the tests, there were some liquid left on the bottom of the quartz tube. As the pressure decreased, the amount of liquid increased.

4.2.1.2 Test Results for Pressures Higher than 8.8 MPa:

For tests in this pressure range, the bubble size decreased to an indiscernible level, resulting a flat reacting surface. Unlike tests in the previous pressure range, no clear brown gas was observed on top of the dark-colored cloud; instead, the dark-colored cloud filled up the whole tube above the reacting surface. It was most likely that as the pressure exceeded a threshold, a change of reaction mechanism happened and accelerated the generation of dark-colored cloud. This corresponded to a rapid increase of the burning rate as described in next section. Right after the front reached the bottom of the tube and the whole column of liquid was depleted, the dark cloud turned into transparent gases, which was similar to the phenomena of XM46 combustion at pressures below 28 MPa.

4.2.2 Burning Rate vs. Pressure Correlation

The burning rate as a function of pressure up to 14.5 MPa is shown in Figure 10 together with the burning rate of XM46 at the same pressure range. As seen in the figure, the burning rate can be fitted into four power law regions. An extremely high pressure-exponent of 5.5 was observed between 8.8MPa and 12.2 MPa, and the trend seemed to level off beyond 12.2 MPa. At pressures below 8.8 MPa, the burning rate of XM46 is roughly two order-of-magnitude higher than that of Primex propellant, however, the difference shrinks to about five times at pressure around 13 MPa.

4.2.3 Combustion Zone Structure Measured by Microthermocouple

Temperature distributions inside the reaction zone were measured using 25-μm S-type thermocouples. Typical temperature traces corresponding to each of the burning rate region described in the above paragraph were shown in Figure 11. For pressures between 1.5 and 2.8 MPa (Figure 11(a), P = 2.1 MPa), once the front reached the thermocouple, the temperature rose to a temperature slightly higher than the boiling point of the water at the chamber pressure, then dropped back to the boiling point. This is a confirmation of the visual observation that the dark cloud consists of both gas and liquid phase. However, in the region close to the regressing front,

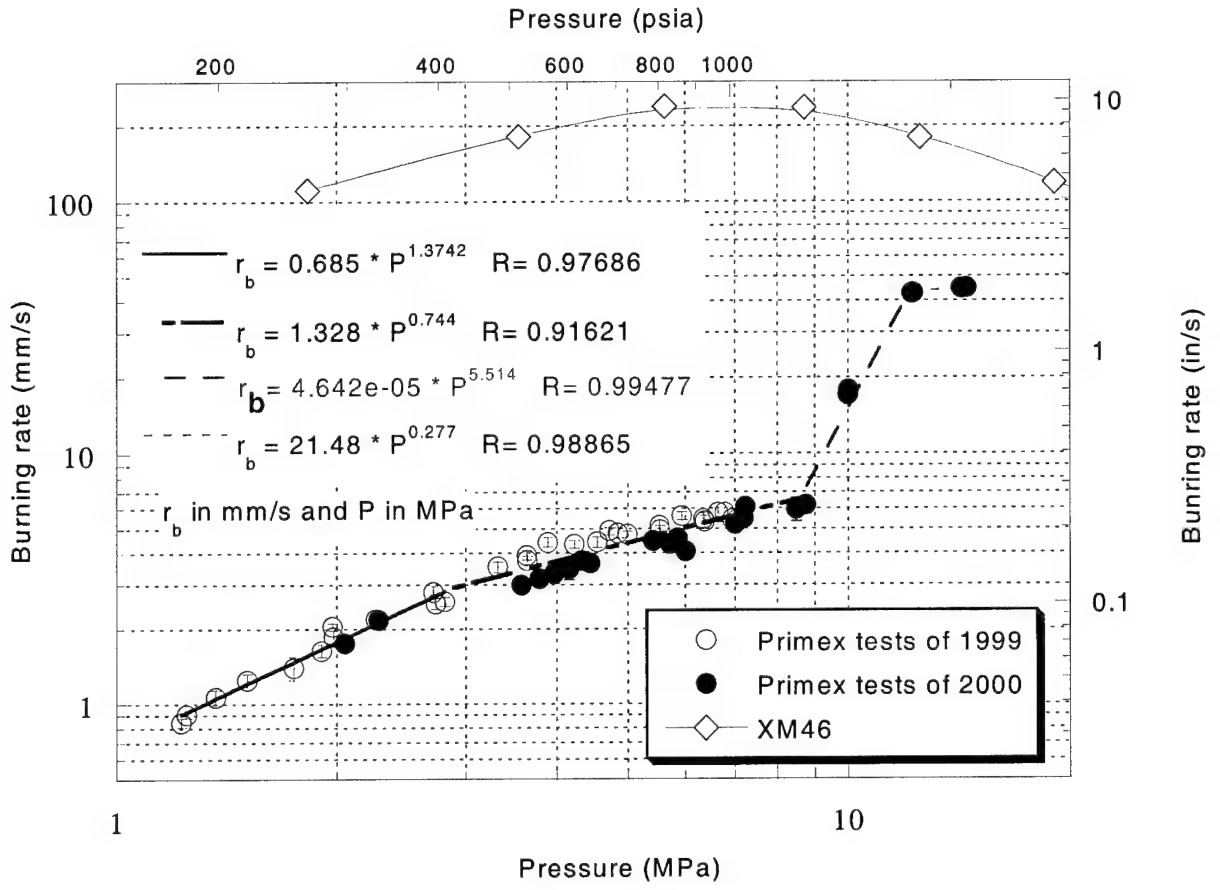

Figure 10. Burning rate comparison between XM46 and Primex propellant.

fluctuations of high frequency were observed. Since the trace before and after this region did not have extensive fluctuation, the possibility of outside noise was ruled out. It is probably due to both the bubbling process and the ions generated in condense phase reactions. Because of the fluctuations, the surface temperatures could not be defined very well.

There was no significant distinction between the temperature traces in the pressure range discussed in the previous paragraph and that between 2.8 and 8.8 MPa. As the pressure increased, the temperature overshoots above the boiling point of the water increased (see Figure 11(b)), so did the length of the region with high-frequency fluctuation.

In the pressure range between 2.8 and 12.2 MPa, the characteristics of the temperature traces changed significantly. As shown in Figure 11(c), the high-frequency fluctuation of temperature trace extended to the sixth second, then it diminished with a second temperature rise observed. Compared to the video record, the second temperature rise corresponded to the conversion of dark-colored cloud into transparent gases after the whole column of liquid was consumed by the regressing front. Therefore, this high-frequency fluctuation section of trace corresponded to the temperature of dark-colored smoke in the tube. From Figure 11(c), the temperature did not exceed the boiling point of water most of the time in this period. It suggested that, although the dark-colored cloud was most likely to be a two-phase mixture, the condensed-phase reactions were dominating.

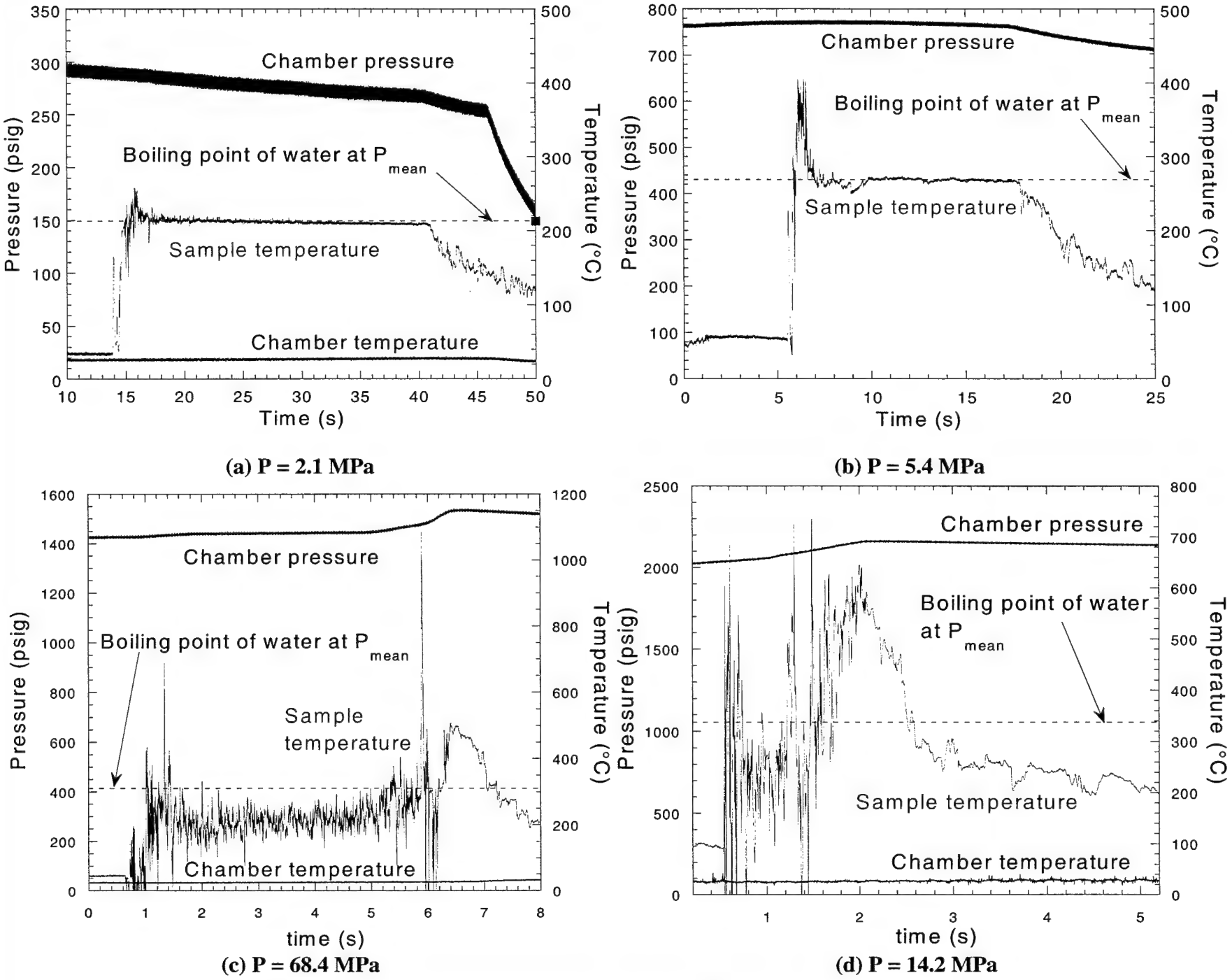

Figure 11. Typical temperature traces at different pressure ranges.

Based upon the available data, the temperature trace for tests at pressures above 12.2 MPa seemed to be similar to those at pressure range between 8.8 and 12.2 MPa. Figure 11(d) shows the temperature trace measured at 14.2 MPa. The period of high-frequency fluctuation was shorter because of higher regression rate. The amplitude of the fluctuation was somewhat higher than that of Figure 11(c).

5 Discussion of Results

5.1 Staged Nature of HAN-based Propellant Combustion

As mentioned in the introduction and seen in the present study, XM46 liquid propellant exhibits staged combustion characteristics. It was proposed in the literature[10,14] that in the reaction zone, HAN decomposed first, followed by a region with mixed HAN decomposition products and dispersed molten TEAN droplets; then the TEAN decomposed and reacted with HAN decomposition products producing a luminous flame. This interpretation, however, has difficulty explaining other phenomena reported in the literature, such as early appearance of carbon-containing species for high heat-flux laser heating experiments.[12] Therefore, one should consider the possibility of the simultaneous TEAN decomposition with HAN. Furthermore, the results from this study on XM46 strongly suggest that TEAN decomposes nearly simultaneously with HAN. As shown in Figure 7, carbon-containing species were observed in the gas evolved from the XM46 sample heated to 130 °C, which is below the HAN decomposition temperature of 160 to 170 °C. The minimum temperature of 130 °C for observing carbon-containing species is also lower than the TEAN decomposition temperature around 240 to 250 °C.[5]

From the measured temperature plateau around 300 °C at pressures up to 17.5 MPa, it can be postulated that the reaction rates in the dark-smoke zone are extremely slow. Since this temperature is higher than the reported TEAN decomposition temperature, it is most likely that there are no intact TEAN molecules in the dark-smoke region.

Another piece of evidence for simultaneous decomposition of TEAN and HAN is the very dark color of the product gases generated from the decomposition reactions. Among many decomposition species of HAN, NO_2 is the only significant source of color, a brown-colored gas. The dark-colored smoke must have substantial contribution from TEAN decomposition products, since TEAN is the only carbon-containing component of XM46. Based upon the above observation and interpretation, it is a logical deduction that TEAN also participates actively in the initial decomposition stage of XM46.

From the above reasoning, it is proposed that the reaction of XM46 consists of the following steps:

a) The initial decomposition of both HAN and TEAN is most likely initiated in the liquid phase, since the temperature gradients in liquid and gas phases are extremely steep and the temperature of the gaseous decomposition products very close to the surface is around 300 °C, which is significantly higher than the observed initial decomposition temperature of 130

°C. The decomposition products are believed to include brown-colored NO_2 and heavy intermediate opaque carbon-containing species.

b) At low pressures (below 28 MPa), heavy intermediate species can have long residence time before breaking down into transparent molecules. This causes formation of a thick dark-opaque zone above the burning surface. As pressure increases, the residence time decreases, resulting in the reduction of the height of the dark-opaque zone. At around 600 °C, all NO_2 and carbon-containing opaque intermediate species have been converted into transparent species.

After a short induction period, the reaction between transparent species can produce a steep temperature gradient associated with the appearance of a luminous flame. The duration of the induction period is also a function of pressure. At very high pressures, the two steep temperature regions can even coalesce into a single temperature jump region.

5.2 Mechanism of Flash-back Phenomenon

In the initial feeding tests, the feeding piston was advanced in a stepped motion. In this mode, the controller allowed the feeding rate to be adjusted during the test. It was initially believed that the resulting pulsating nature of the liquid surface was the cause for the continued burn back of the LP. Systems were designed to dampen the pulsation of the surface. One such design utilized two relatively large reservoirs mounted in parallel with the burning tip. Another design was to feed the LP by gravity from the two side reservoirs to the central tube resulting in smooth upward feeding of the propellant. It also provided a discontinuity between the stored propellant for combustion and the propellant in the supply lines to prevent burn back into the feeding apparatus. These designs did not, however, prevent the flame from regressing and propagating into the two reservoirs and the supply lines.

All subsequent tests were conducted using a constant-rate feeding mode of the piston. One disadvantage of this mode is that the feeding rate cannot be adjusted during the test. In order to maintain the LP surface at a fixed position, the chamber pressure was to be adjusted during the test. However, the burn back-event was too rapid for altering the chamber pressure. Tests were performed using feeding rates as high as 35.5 cm/s; yet even at such high feeding rates, the burn-back phenomenon still occurred.

It was also considered that the continued burn-back could be caused by increased heat feedback from the tube walls. To examine this possibility, end sections of the feeding tubes were fabricated from materials with lower thermal conductivity than quartz, including Pyrex and a high-temperature carbon phenolic ablative material, MXB360. When these sections did not resolve the problem of burn-back, an actively cooled tip utilizing a water flow was constructed. With these changes having no impact on the burn-back problem, heat feedback from the tube walls was ruled out as the major cause of the continued regression into the feeding tube. The main reason for burn-back is therefore believed to be the liquid-phase reactions enhanced by surface agitation. This subsurface reaction could be suppressed by several methods, including the increase of LP viscosity, the replacement of TEAN with a more reactive compound which can react in a more compatible manner with HAN, or the use of catalysts to promote surface and gas-phase reactions.

5.3 Controlling Parameters of Combustion

The mechanism through which the pressure affects the burning rate of XM46 is not totally understood. However, some possible controlling mechanisms have been identified after reviewing the results of this investigation together with existing literature.

HAN-water solution, when heated, is known to undergo a series of liquid-phase reactions, as summarized by Lee and Thynell.[4] Therefore, it is reasonable to assume that the decomposition front of XM46 combustion is initiated and controlled by liquid phase reactions. However, the pressure does not directly affect the species concentrations in the liquid phase. Therefore, pressure affects the burning rate in an indirect manner.

Some possible mechanisms through which the pressure affects the burning rate of XM46 are: (1) increasing gas phase heat release rate with increasing pressure; (2) increasing gas-phase heat conduction, and thus heat feedback, with increasing pressure; (3) decreasing latent heat of water with increasing pressure; and (4) increasing gas dissolution rate or decreasing gas desorption rate with increasing pressure. Mechanisms (1) and (2) are generally tied together, because the heat release in the gas phase provides the energy for conductive heat transfer back to the unburned propellant. Unlike the conventional propellant combustion situation, the burning rate of the propellant is a highly nonlinear function of pressure due to its dependency on multiple parameters, including: the pressure dependent latent heat of water, ΔH_v, (see Figure 12), the enthalpy increase from initial to surface temperature, the conductive heat flux from the gas phase, $\dot{q}''_{cond}$, the net radiative heat flux absorbed at the surface, $\dot{q}''_{rad}$, and the heat release in the surface layer, Q_s, as shown by the following simplified energy flux balance equation across the gas/liquid interface:

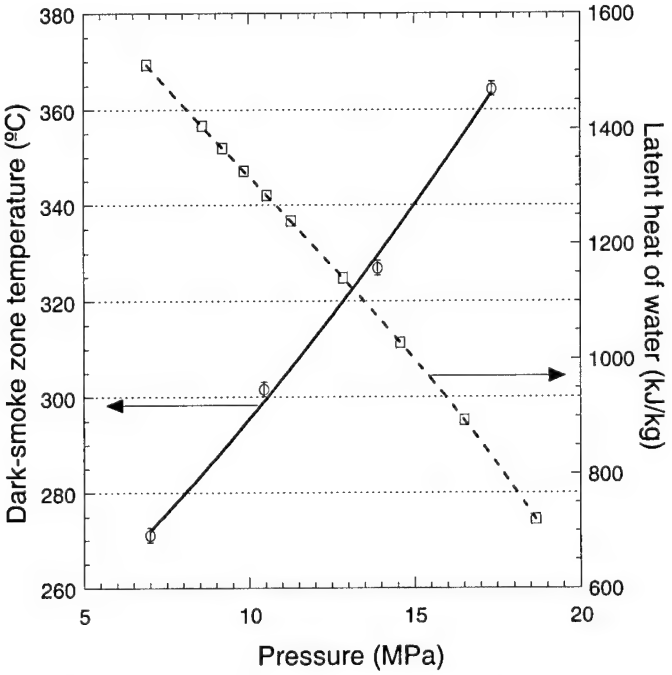

Figure 12. Variation of dark-smoke temperature and latent heat of water with pressure.

$$\rho_p r_b \left(\int_{T_i}^{T_s} C_p dT + \Delta H_v \right) = \rho_p r_b Q_s + \dot{q}''_{cond} + \dot{q}''_{rad} + \sum_{i=1}^{N} \rho_p Y_{i-} V_{i-} \Delta h^{\circ}_{f,i-} - \sum_{i=1}^{N} \rho_{g+} Y_{i+} V_{i+} \Delta h^{\circ}_{f,i+}$$

where ρ_p is the propellant density, r_b the burning rate, C_p the averaged constant-pressure specific heat, and Y_i, V_i the mass fraction, the diffusion velocity of i-th species, respectively. Subscripts "+" and "–" denote the position just right above or below the interface. At higher pressures, the liquid surface temperature is higher based upon the observed trend of the dark-smoke zone temperature shown in Figure 12. It should be noted that the measured dark-smoke zone temperature is not exactly the surface temperature. However, the surface temperature should follow a similar trend, based upon the temperature continuity requirement at the gas/liquid interface.

As shown in Figure 12, the latent heat of water decreases with increase in pressure. The temperature of the dark-smoke zone increased more than 80 °C with increasing pressure in the range from 7 to 17.5 MPa. Since the dark-smoke zone temperature increases with pressure, the enthalpy difference from the initial temperature to the surface temperature should also increase with pressure. The value of Q_s should increase with pressure. As pressure is increased, the temperature within the surface reaction zone increases, thereby promoting the reaction of the decomposition species in the liquid, as well as increasing the collision rate and the heterogeneous reaction rate of gas-phase molecules on the liquid surface. In addition, both the conductive heat flux from the gas phase and the net radiative heat flux absorbed at the surface are functions of pressure. Therefore, Eq (1) is a highly nonlinear pressure-dependent equation; the burning rate determined from this complex relationship can vary with pressure in a non-conventional manner.

As pointed out by Harting et al.,[13] the evaporation of water can play an important role in HAN-based liquid propellants. The heat released during HAN and TEAN decomposition has to vaporize the water and to increase the sensible enthalpy of the combustion products. Due to the decrease of the latent heat of water with pressure, the sensible enthalpy of the products will be higher. According to the CEA calculation, the total heat of reaction of XM46 combustion is 5,116 kJ/kg. However, much of the energy is released in the gas phase region away from the decomposition front. Therefore, the latent heat of water (1,551 kJ/kg at 6.9 MPa) can be a significant portion of the heat release in the decomposition zone.

Another point worth noting is that the activation energy of solid HAN (47.12 kJ/mol)[4], solid TEAN (68.5 kJ/mol)[6], and the latent heat of water converted to a molar basis (40.63 kJ/mol at 1 atm) are all on the same order of the magnitude. Therefore, the change in the latent heat of water can affect the balance between decomposition and evaporation processes. Other physical processes can also play a role in the burning rate trend of XM46. Surface instability has been identified as one of the controlling mechanisms of the liquid propellant apparent burning rates.[14] The decrease of burning rate as pressure was increased from 7 to 28 MPa can be attributed to the suppression of the surface ripples as the gas/liquid density ratio across the interface increased. However, it is hard to explain the burning rate trends observed at other pressure ranges in this study using the surface instability interpretation alone.

The gas dissolution/desorption process can also affect the burning rate in different ways. First, the dissolution of some gas species could generate radicals to accelerate reactions. For example,

the dissolution of NO_2 in water can generate nitrous acid,[15] which is known to enhance the HAN decomposition reactions:

$$2NO_2 + H_2O \rightarrow HNO_2 + HNO_3 \qquad \textbf{(R 15)}$$

Second, as pressure increases, the product concentration in the gas phase becomes higher; this increases the probability for product gas dissolution gas into the liquid phase, which in turn could retard the forward reaction.

From Figure 10, the burning rate of Primex propellant was found to be two orders of magnitude lower than that of XM46 for $P < 8.8$ MPa. Therefore, if the thermal diffusivity of Primex propellant is on the same order of magnitude as the thermal diffusivity of XM46, the thermal wave thickness of the Primex propellant would be much thicker than that of the burning XM46. However, as observed in temperature traces of Primex propellant tests, the thermal wave is extremely thin, and the preheating zone near the burning surface could not be easily analyzed.

Instead of heat-feedback from the gas phase, chemical species diffusion could be the controlling process of the regression front propagation. Similar to the premixed laminar gaseous flame[16], the diffusion process could control the regression rate. The situation here is more complex. The existence of a two-phase region above the regression front suggests that the front propagation is controlled by condensed phase reaction, and is driven by condensed phase diffusion. As well described in the literature[3,4,7,8], HAN decomposition has autocatalytic characteristics, with nitrous acid serving as the catalyst. As given in Section 3, nitrous acid accelerates the decomposition of HAN. Moreover, HAN decomposition can be initiated with sufficient amount of NO_2 in the surrounding,[2] which generates nitrous acid when it is dissolved into water.[15] The reaction mechanism (R 9) as summarized by Thynell also shows the possibility of reaction initiation by nitrous acid without external heat source. Since the reaction could be accelerated, even initiated by one of the decomposition products, it is plausible that the concentration gradient of one or more species could be the driving force of the front propagation.

5.4 Effect of Fuel Component

Since TEAN also participates in the decomposition reaction, the fuel component can play an important role in the early stage of the combustion event. Since the weight fractions of HAN and water Primex propellant are comparable with those in XM46, the only significant change is the replacement of TEAN by glycine. With the data of Primex propellant, one can study the effect of fuel component. The burning rate was found to be significantly lower than that of XM46. Based upon limited feeding test results, the flashback phenomenon was also significantly altered with the change of fuel component. It is quite evident that the type of fuel ingredient in the HAN-based liquid propellants can strongly affect the major combustion characteristics.

6 Summary

Based upon the experimental observations and measurements, several important conclusions are summarized below.

1. XM46 exhibits some unconventional characteristics, such as flashback behavior and negative pressure exponent. The characteristics are believed to be caused by the complex physical and chemical process occurs in condense phase region.
2. The intrinsic burning rates of XM46 measured with combustible straws increase with pressure when $P < 7$ MPa, decrease with pressure when $7 < P < 28$ MPa, exhibit a hump-like shape when $28 < P < 80$ MPa, and increase again when $P > 80$ MPa. The luminous flame was observed only when the pressure is above 28 MPa.
3. TEAN participates in the decomposition reactions of XM46 initiated in the liquid phase, producing dark-colored gaseous products (including NO_2 and large carbon containing species) at temperatures around 300 °C
4. Pyrolysis tests of XM46 were conducted in a specially designed pyrolyzer used in conjunction with a gas chromatograph/mass spectrometer. The major pyrolysis products observed were NO, N_2O, N_2, CO_2, CO, H_2O, HCN, and C_2H_4 when pyrolyzed at temperatures between 130 and 540 °C.
5. A number of physicochemical processes which could have significant influence on burning characteristics of the HAN-based liquid propellant was considered. Unlike the conventional solid propellant combustion situation, the pressure dependency of the burning rate of the HAN-based liquid propellant cannot be represented by a simple function. Water evaporation below the critical point seems to have a noticeable effect on combustion characteristics of XM46, since the latent heat is on the same order of magnitude with HAN and TEAN activation energy and the amount of heat release in the decomposition zone. Gas dissolution/desorption could also affect the burning rate. From the temperature traces measured from slower-burning Primex propellant, the chemical species diffusion process of certain products, such as nitrous acid could play an important role in controlling the rate of regression front propagation. These species can introduce autocatalytic reaction effects in HAN-based solutions.
6. The type of fuel ingredient in HAN-based liquid monopropellant has a significant effect on the overall burning characteristics, as demonstrated by the replacement of TEAN with glycine.

List of Publications

Jennings, S.T., Chang, Y.P, Koch, D., and Kuo, K. K., "Peculiar Combustion Characteristics of XM46 Liquid Propellant," Proceedings of the 34th JANNAF Combustion Subcommittee Meeting, West Palm Beach, FL, *CPIA Publication 662*, Volume I, pp. 321-333, October, 1997.

Boyer, E., Koch, D., Kuo, K. K., and Lu, Y.C., "Intrinsic Burning Rate and Temperature Sensitivity of Nitromethane," Proceedings of the 34th JANNAF Combustion Subcommittee Meeting, West Palm Beach, FL, *CPIA Publication 662*, Volume I, pp. 335-346, October, 1997.

Lu, Y.C., E. Boyer, D. Koch, and K.K. Kuo, "Measurement of Intrinsic Burning Rate of Nitromethane," AIAA Paper No. 97-3107, 33rd AIAA/ASME/SAE/ASEE Joint Propulsion Conference, Seattle, WA, July 6-9, 1997.

Challenges in Propellants and Combustion 100 Years After Nobel, editor Kenneth K. Kuo and 9 associate editors, Begell House Inc., 1181 pages, August, 1997.

Chang, Y.P., Boyer, E., Yeh, C. L., Kuo, K.K., and Jennings, S.T., "Combustion Behavior of XM46 Liquid Propellant," *24th International Pyrotechnics Seminar,* Monterey, CA, July 27-31, pp. 625-635, 1998.

Boyer, E. and Kuo, K. K., "Flame Structure and Combustion Behavior of Nitromethane," *35th JANNAF Combustion Subcommittee Meeting*, Tucson, AZ, December 7-10, 1998.

Boyer, E. and Kuo, K. K., "High Pressure Combustion Behavior of Nitromethane," AIAA Paper 99-2358, 35th AIAA/ASME/SAE/ASEE Joint Propulsion Conference, 20-24 June 1999, Los Angeles, CA.

Chang, Y.-P., Boyer, E., and Kuo, K. K., "Combustion Behavior And Flame Structure Of Xm46 Liquid Propellant," AIAA paper 2000-0706, 38th Aerospace Sciences Meeting & Exhibit, 10-13 January 2000, Reno, NV.

List of Scientific Personnel

Participating

Kenneth K. Kuo, Distinguished Professor and Director of the High Pressure Combustion Laboratory
Yi-Ping Chang, Ph.D. Candidate
Eric Boyer, Ph.D. Candidate
Stephen T. Jennings, Masters Student
Chun-Liang Yeh, Research Associate
Donald E. Koch, Research Assistant

Degrees Awarded

Stephen T. Jennings, Master of Science in Mechanical Engineering, December, 1997.

References

[1] Klein, N., "Ignition and Combustion of the HAN-Based Liquid Propellants," 27th JANNAF Combustion Subcommittee Meeting, Vol. 1, pp. 443—450, 1990.

[2] Carleton, F. B., Klein, N., Krallis, K. and Weinberg, F. J., "Laser Ignition of Liquid Propellants," 23rd Symposium (International) on Combustion, pp. 1323—1329, 1990.

[3] Schoppelrei and Brill, T. B., "Spectroscopy of Hydrothermal Reactions. 7. Kinetics of Aqueous $[NH_3OH]NO_3$ at 463—523 K and 27.5 MPa by Infrared Spectroscopy," Journal of Physical Chemistry, Vol. 101, pp. 8593—8596, 1997.

[4] Lee, H. S. and Thynell, S. T., "Confined Rapid Thermolysis/FTIR Spectroscopy of Hydroxylammonium Nitrate," AIAA Paper 97-3232, 33rd AIAA/ASME/SAE/ASEE Joint Propulsion Conference & Exhibit, Seattle, WA, 1997.

[5] Cronin, J. T. and Brill, T. B., "Thermal Decomposition of Energetic Materials 29 – The Fast Thermal Decomposition Characteristics of a Multicomponent Material: Liquid Gun Propellant 1845," Combustion and Flame, Vol. 74, pp. 81-89, 1988.

[6] Beyer, R. A., "Shock Tube Study of the Reaction of Triethanol Ammonium Nitrate with N_2O," 27th JANNAF Combustion Meeting, CPIA Pub. 557, Vol. 1, pp. 605—609, Nov. 1990.
[7] Schoppelrei, J. W., Kieke, M. L., and Brill, T. B., "Spectroscopy of Hydrothermal Reactions. 2. Reactions and Kinetic Parameters of $[NH_3OH]NO_3$ and Equilibria of $(NH_4)_2CO_3$ Determined with a Flow Cell and FT Raman Spectroscopy," Journal of Physical Chemistry, Vol. 100, pp. 7463—7470, 1996.
[8] Thynell, S. T. and Kim, E. S., "The Effect of Pressure on the Thermal Decomposition Characteristics of Hydroxylammonium Nitrate," 35th JANNAF Combustion Subcommittee Meeting, pp. 47—59, 1998.
[9] McBratney, W. F. and Vanderhoff, J. A., "High Pressure Windowed Chamber Burn Rate Determination of Liquid Propellant XM46," ARL Report ARL-TR-442, Army Research Lab, Aberdeen, MD, 1994.
[10] Vosen, S. R., "Hydroxylammonium Nitrate-Based Liquid Propellant Combustion – Interpretation of Strand Burner Data and the Laminar Burning Velocity," Combustion and Flame, Vol. 82, pp. 376-388, 1990.
[11] Chang, Y. P., Boyer, E., Yeh, C. L., Kuo, K. K., and Jennings, S. T., "Combustion Behavior of XM46 Liquid Propellant," 24th International Pyrotechnics Seminar, Monterey, CA, July 27-31, pp. 625-635, 1998.
[12] Lee, Y. J. and Litzinger, T. A., "Combustion Chemistry of HAN, TEAN, and XM46," Combustion Science and Technology, Vol. 141, pp. 19-36, 1999.
[13] Harting, G. C., Mordosky, J. W., Zhang, B. Q., Cook, T. T., and Kuo, K. K., "Burning Rate Characterization of OXSOL Liquid Oxidizer," 36th JANNAF Combustion Subcommittee Meeting, Cocoa Beach, FL, Oct. 18-22, 1999.
[14] Vosen, S. R., "Concentration and Pressure Effects on the Decomposition Rate of Aqueous Hydroxylammonium Nitrate Solutions," Combustion Science and Technology, Vol. 68, pp. 85-99, 1989.
[15] Leveritt, C. S., Bunte, S. W., and Klein, N., "Hydroxylammonium Nitrate (HAN) Liquid Propellant Stability Enhancement," ARL-TR-2037, Army Research Laboratory, Aberdeen Proving Ground, MD, September 1999.
[16] Kuo, K. K., "Principles of Combustion," Chapter 5, p. 298, John Wiley & Sons, 1986.